Camera selection for real-time *in vivo* radiation treatment verification systems using Cherenkov imaging

Jacqueline M. Andreozzi[a)]
Thayer School of Engineering, Dartmouth College, Hanover, New Hampshire 03755

Rongxiao Zhang
Department of Physics and Astronomy, Dartmouth College, Hanover, New Hampshire 03755

Adam K. Glaser
Thayer School of Engineering, Dartmouth College, Hanover, New Hampshire 03755

Lesley A. Jarvis
Department of Medicine, Geisel School of Medicine and Norris Cotton Cancer Center, Dartmouth-Hitchcock Medical Center, Lebanon, New Hampshire 03766

Brian W. Pogue[a)]
Thayer School of Engineering and Department of Physics and Astronomy, Dartmouth College, Hanover, New Hampshire 03755

David J. Gladstone
Department of Medicine, Geisel School of Medicine and Norris Cotton Cancer Center, Dartmouth-Hitchcock Medical Center, Lebanon, New Hampshire 03766

(Received 3 September 2014; revised 5 January 2015; accepted for publication 7 January 2015; published 29 January 2015)

Purpose: To identify achievable camera performance and hardware needs in a clinical Cherenkov imaging system for real-time, *in vivo* monitoring of the surface beam profile on patients, as novel visual information, documentation, and possible treatment verification for clinicians.
Methods: Complementary metal-oxide-semiconductor (CMOS), charge-coupled device (CCD), intensified charge-coupled device (ICCD), and electron multiplying-intensified charge coupled device (EM-ICCD) cameras were investigated to determine Cherenkov imaging performance in a clinical radiotherapy setting, with one emphasis on the maximum supportable frame rate. Where possible, the image intensifier was synchronized using a pulse signal from the Linac in order to image with room lighting conditions comparable to patient treatment scenarios. A solid water phantom irradiated with a 6 MV photon beam was imaged by the cameras to evaluate the maximum frame rate for adequate Cherenkov detection. Adequate detection was defined as an average electron count in the background-subtracted Cherenkov image region of interest in excess of 0.5% (327 counts) of the 16-bit maximum electron count value. Additionally, an ICCD and an EM-ICCD were each used clinically to image two patients undergoing whole-breast radiotherapy to compare clinical advantages and limitations of each system.
Results: Intensifier-coupled cameras were required for imaging Cherenkov emission on the phantom surface with ambient room lighting; standalone CMOS and CCD cameras were not viable. The EM-ICCD was able to collect images from a single Linac pulse delivering less than 0.05 cGy of dose at 30 frames/s (fps) and pixel resolution of 512×512, compared to an ICCD which was limited to 4.7 fps at 1024×1024 resolution. An intensifier with higher quantum efficiency at the entrance photocathode in the red wavelengths [30% quantum efficiency (QE) vs previous 19%] promises at least 8.6 fps at a resolution of 1024×1024 and lower monetary cost than the EM-ICCD.
Conclusions: The ICCD with an intensifier better optimized for red wavelengths was found to provide the best potential for real-time display (at least 8.6 fps) of radiation dose on the skin during treatment at a resolution of 1024×1024. © *2015 American Association of Physicists in Medicine.* [http://dx.doi.org/10.1118/1.4906249]

Key words: Cerenkov, Cherenkov, image, dosimetry, visualization, therapy

1. INTRODUCTION

This paper explores the hardware requirements for Cherenkov imaging during radiation therapy, a newly emerging modality of *in vivo* radiotherapy monitoring which can display an optical analog for the treatment beam on the patient in real time. Where other types of luminescence imaging capture Cherenkov photons generated from injected radionuclides (molecular imaging),[1] the examined approach focuses on detecting the Cherenkov photons produced from the interaction of high energy x-ray beams with surface tissue.

The relevance of this imaging is as related to current clinical methods of treatment verification, which have the overall goal of achieving precise and accurate dose delivery through pretreatment quality assurance (QA) and patient alignment protocols. These current methods are assumed to be robust on the grounds that careful QA and alignment provides an implicit direct relationship between the planned treatment and the delivered dose. Various techniques of *in vivo* dosimetry and treatment verification have been investigated to provide on patient verification of delivery, as well as to provide a more dependable means of permanent treatment records.[2]

The range of "on patient" measurement systems varies considerably in technology. Thermoluminescent detectors (TLDs) are perhaps the most common form of *in vivo* dosimeters implemented regularly in the clinic. However, as point measurements that do not give real-time feedback, the usefulness of TLDs is limited to cases where an immediately passive role is suitable such as in the case of posttreatment dose verification.[3–8] To provide more direct and immediate information, many groups have investigated the use of 2D, 3D, and even 4D electronic portal imaging device (EPID) reconstructions of dose fluence.[9–17] Major strides have been made with this technology, but routine use in everyday fractionated delivery has not yet occurred due to some unresolved issues.[18]

In addition to quality assurance,[19] Cherenkov imaging is being examined for *in vivo* surface dosimetry and beam tracking for real-time treatment verification.[20,21] As a passive monitoring modality, Cherenkov imaging would neither require any further dose to the patient nor interfere with typical treatment protocols. Initial studies on the applications of Cherenkov imaging have shown feasibility of imaging repeatedly, and studies of the potential medical value are ongoing.[22,23]

Because Cherenkov emission is a low intensity photon signal spanning the entire optical spectrum, the successful realization of this in a clinical setting would require several key criteria to be met by the hardware. There are three critical components of the clinical environment in this regard. First, the emission from human tissue is attenuated by absorption and scatter, as compared to water emission, so the camera must have sufficient gain to image a low light level. Second, the system must be able to capture this signal in the midst of ambient room light at levels typically used for patient safety and comfort.

Finally, to be viable as a tool at monitoring and detecting deviations from the planned treatment in real-time, especially in dynamic therapies such as IMRT or VMAT, the rate at which the camera captures and displays the information must approach video frame rates (5–30 fps).[24] By monitoring the beam in real-time, irregular beam deliveries which manifest as abnormal beam shapes (from patient misalignment and multileaf collimator malfunction) or uncharacteristic intensities (improper beam accessories) could be detected. Several camera systems were tested and assessed based on these criteria*: (i) low light sensitivity, (ii) background light suppression, and (iii) fast frame rate*, in order to identify the best candidates for clinical Cherenkov imaging.

Based on previous experiences, our hypothesis was that real-time clinical Cherenkov imaging of patients for treatment verification would require a detector equipped with both a high gain mechanism as well as triggered, time-gated acquisition capability. Yet to be thorough in the evaluation, a set of cameras representing the comprehensive possible choices was used, with no gain, with gain, without gating, and with gating. Comparison analysis was completed with average intensity values from images of a standard phantom, using a simple phantom in the same treatment and imaging geometry. Finally, the two high performing choices of cameras were compared directly in images taken during the first clinical trial of Cherenkov imaging during radiotherapy as a standard of comparison for the other imaging systems.

2. MATERIALS AND METHODS

2.A. Cameras

The five cameras listed in Table I were investigated in this study to determine metrics of performance at Cherenkov imaging under clinically relevant conditions. Each of the four types of cameras represented, charge-coupled device (CCD), complementary metal-oxide-semiconductor (CMOS), intensi-

TABLE I. Key performance specifications of the five cameras examined as possible detectors for clinical Cherenkov imaging. For the PIMAX cameras, the image intensifier is specified as either Gen2 or Gen3 in the sensor type.

Sensor type	Camera model	Approx cost	Chip size (mm)	Pixel size (μm)	Sensor size (pixels)	Gain factor	Gate time (ns)	QE of detector @ 700 nm (%)	QE of intensifier @ 700 nm	Max frame rate
CMOS	Canon EOS rebel T3i	\$600	22.3 × 14.9	4.3	5184 × 3456	1	N/A	≈25–40	N/A	3.7
CCD	Apogee alta F8300	\$3k	18 × 13.5	5.4	3326 × 2504	1	N/A	42	N/A	0.1
ICCD (Unigen2)	PIMAX3 1024i	\$55k	13.1 × 13.1	12.8	1024 × 1024	100	2	27	19%	27
ICCD (HRf)	PIMAX4 1024i	\$60k	13.1 × 13.1	12.8	1024 × 1024	100	2	27	30%	27
EM-ICCD (HRf)	PIMAX4 512EM	\$85k	8.0 × 8.0	16.0	512 × 512	10 000	2	46	30%	30

fied charge-coupled device (ICCD), and electron multiplying-intensified charge coupled device (EM-ICCD), has its own inherent strengths and weaknesses. Again, the key factors in the evaluation here were related to: (i) low light sensitivity or detective quantum efficiency (DQE), (ii) ambient light rejection, which is solved by gated intensified acquisition typically, and (iii) frame rate capability. Still of the available options, there are many nuances to the specifications, which will be briefly discussed below. Table I lists specifications which the researchers identified as the most meaningful indicators of Cherenkov imaging performance.

Cost can be a prohibitive factor in realizing any novel modality (imaging or otherwise), and as such, it was deemed necessary to take into consideration during the evaluation. Low cost was one motivation for including the CMOS and CCD camera options in this study along with their comparatively high quantum efficiency (QE) values. The monetary values shown in the table reflect figures quoted at the time but could vary by a factor of 2 depending upon manufacturer and specifications. The consequences of overall resolution, and the constituent chip and pixel sizes, were left as qualitative factors to be discussed with reference to the clinical images acquired for this study.

The ability to time gate image acquisition down to 3–5 μs intervals is an important ability inherent in the intensified cameras, since the emission of Cherenkov photons is limited to the small time gap immediately after the radiation pulse enters the tissue.[25] The intensifier itself is able to act as a fast optical switch that activates when Cherenkov emission is expected. Results shown in Sec. 3.A from the first two cameras listed in Table I will further illustrate this ability.

Cherenkov emission has a continuous wavelength spectrum heavily weighted in the blue, but because tissue absorbs light in these spectral regions, the detected Cherenkov emission from the surface of the patient is predominantly in the red and near-infrared region.[26–29] The quantum efficiency of the detectors and intensifiers at 700 nm is subsequently valuable in Table I as a metric for comparing sensitivity to Cherenkov emission from tissue. It is important to point out that mismatch between the Cherenkov emission spectrum and the spectral response (quantum efficiency curve) of the detection hardware will influence the perceived intensity of the imaged Cherenkov light. Success in Cherenkov imaging requires thoughtful hardware selection in this regard.

Two ICCDs were compared to evaluate the effect of the different intensifier characteristics. The intensifiers are the sole gain mechanism of these two cameras. Incoming optical photons are incident on the photocathode and converted to electrons. These electrons are then accelerated and multiplied in the noise-free vacuum of the micro-channel plate amplifier, and then the amplified electron signal is converted back to optical photons using an output phosphor screen at the back of the intensifier. The photons generated in the phosphor screen are then imaged by the CCD detector as the recorded image.

The gain offered by the intensifier serves to diminish the effect of readout noise and shot noise in the final images, since the latter noise sources become relatively small in comparison to the amplified average signal. One drawback in the proposed application is the amplification of noise from stray radiation photons can occur leading to high singular point "salt-and-pepper noise" in the Cherenkov photon signal. However, the image processing methods of primarily temporal median filtering described in this paper sufficiently remove both natural (CCD, CMOS) and amplified (ICCD, EM-ICCD) salt-and-pepper noise.

Each model intensifier has a wavelength-dependent spectral response (provided from the manufacturer as quantum efficiency curve) based on the sensitivities of the photocathode. Not only does the phosphor screen efficiency vary between tubes but there is also an efficiency associated with the optical coupling of the components, in addition to each CCD also having its own inherent quantum efficiency spectral response. So, all of these factors multiply together to produce the final signal and must be taken into consideration when evaluating ICCD performance.

One of the ICCDs was equipped with a Unigen 2 coated filmless Generation 3 intensifier with a P43 output phosphor (Unigen 2) that has peak spectral response varying between 17% and 19% quantum efficiency in the 500–800 nm range. The Unigen 2 coating extends the spectral response of the intensifier into the UV range, while being transparent and having no effect in the red/infrared regions. The benefit of this coating is limited for imaging Cherenkov in tissue, for the reason described above. The camera design with the Unigen 2 coated intensifier also includes a fiber optic plate, which has a certain loss factor in translating the phosphor image to the CCD.

The Unigen 2 ICCD was the primary imaging system used in the recently concluded first clinical trial of Cherenkov imaging during radiotherapy.[22] Eleven of the twelve whole-breast radiotherapy patients in this trial were imaged with this ICCD, and most of the data were acquired at a frame rate of 4.7 fps. The average Cherenkov intensity measured from the phantom in this study by the Unigen 2 ICCD at 4.7 fps is thus considered the minimum standard for performance comparison.

The second ICCD investigated employed an extended red filmless HRf Generation 3 P43 phosphor intensifier (HRf), which is optimized for a 500–800 nm wavelength range, with a quantum efficiency of over 25% in that region. The higher peak quantum efficiency, coupled with the lack of the fiber optic window between the intensifier and photocathode, promised better signal from the HRf ICCD when compared to the Unigen 2 ICCD. Both cameras have the same CCD chip (Kodak KAI-1003), so overall performance of the HRf camera was expected to exceed that of the Unigen 2 ICCD.

Finally, the EM-ICCD was examined because it presented an attractive prospect for an extremely high-gain system, coupled with the ability to gate the intensifier (also an extended red filmless HRf Generation 3 P43 phosphor intensifier). The EM-ICCD offers two separate gain mechanisms to enhance the incoming signal. First, like the ICCD, the EM-ICCD uses an external intensifier. Second, it has an electron-multiplication mechanism associated with the particular CCD, whereby the already-intensified photon signal is further amplified after optical CCD detection, through a gain register in the detector

electronics. Unlike ICCDs, EM-ICCDs are largely insensitive to readout noise, since the two gain mechanisms allow the incoming signal to dominate by orders of magnitude.

The tested EM-ICCD was equipped with the HRf Generation 3 P43 phosphor intensifier (same as one of the ICCDs) coupled with a CCD97-00 Front Illuminated 2-Phase Electron Multiplying CCD (e2v, Inc., Milpitas, CA). The EM-ICCD was used to image one patient in the 12-patient clinical trial referenced above, in addition to the phantom experiment, to examine the potential for higher frame rate imaging with the enhanced gain.

2.B. Experimental setup

To construct a fair comparison between the detectors, the five cameras were positioned in similar geometries to image a flat, 1 cm thick square of opaque white Plastic Water phantom (CMNC, Nashville, TN) in front of a 4 cm thick block of brown opaque Solid Water phantom (CMNC, Nashville, TN) using the same lens, a Canon EF 135 mm f/2L USM lens (Canon U.S.A., Inc., Melville, NY). The phantom was irradiated by a 6 MV, 10×10 cm photon beam at a dose rate of 600 MUs/min, generated from a Clinac 2100CD linear accelerator (Varian Medical Systems, Palo Alto, CA). As shown in the upper diagram of Fig. 1, the gantry was set to 90° so that the photon beam was perpendicularly incident on the phantom, which was placed upright on the treatment table.

The cameras were positioned to the side of the gantry to image the full expanse of the phantom with a minimal deviation from the beam's eye view to prevent occlusion by the gantry. The white light image in Fig. 1 was captured on the CCD to record the standard camera scope of view, which includes a partial view of the gantry head in the right of the frame. A black sheet was placed on the treatment table when imaging with the intensified cameras to eliminate the effect of reflection from the table surface. To monitor data acquisition in real-time, the cameras were controlled via USB or GigE interfaces with a laptop at the treatment console station just outside of the Linac room.

2.C. Image acquisition and processing

The image acquisition process for each of the cameras varied slightly based on the unique proprietary software interfaces and camera settings inherent to each of detection systems; in general, the manufacturer recommended acquisition software was used for each camera. The group of five cameras is naturally separated into two categories: standalone (CMOS, CCD) and intensified (ICCDs, EM-ICCD) detectors. Both categories were processed slightly differently according to this distinction and the general formatting of the native files, but all raw images captured during data acquisition required postprocessing to elucidate the Cherenkov information following the same conventional method.

The characteristic salt and pepper noise observed in the raw images is caused by stray radiation in the imaging environment and is reliably removed with median filtering.

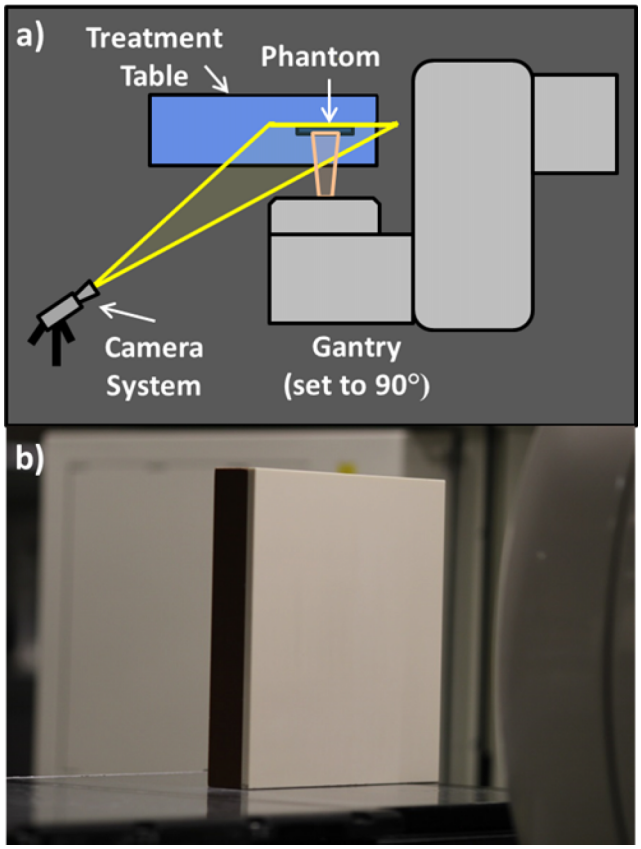

FIG. 1. (a) A top–down view of experimental setup. The gantry was set to 90°, and the radiation beam was incident on the flat solid water phantom positioned vertically on the treatment table. The cameras were placed so as to image the surface of the phantom at an angle without being obstructed by the gantry. (b) For reference, a white light image of the phantom taken on the CCD camera while in position.

Consequently, general processing consisted of application of a temporal median filter across subsequent images, followed by subtraction of a background image to remove any remaining ambient light contributions, and completed by the application of an 11×11 spatial median filter to remove any remaining stray noise.[30] This method also effectively diminishes some of the Poisson or shot noise, since the statistical fluctuations from the detector are reduced in much the same way as the more obvious salt and pepper noise from stray radiation. Background subtraction also serves to remove any bias signal from the detector itself. This postprocessing was carried out in MATLAB (The MathWorks, Inc., Natick, MA).

2.C.1. Standalone detectors: CMOS and CCD

The CMOS camera was operated in single-image acquisition picture mode to exploit the full resolution of the camera (5184×3456). With all room lights turned off, ten images for each of the three test exposures were acquired with the beam on (Cherenkov frames) and three images were also acquired at the same exposure time, but with the beam off to be used as background images, using the software package Canon EOS Utility (Canon U.S.A., Inc., Melville, NY). Three exposure times, 0.1, 1.0, and 3.2 s, were tested. After conversion from RGB color format to grayscale intensity, the set of 13

images corresponding to each of the three exposure times was condensed into a single representative grayscale image. The average of the three background frames was subtracted from the median of the ten Cherenkov frames, and the result was smoothed with an 11×11 spatial median filter, and displayed with an intensity-based colormap for ease of visual interpretation.

In the same manner, a custom LabVIEW (National Instruments Corporation, Austin, TX) program was used to acquire a video stream of ten Cherenkov images and three background images with the radiation beam on and off, respectively, from the CCD. All room lights were turned off when imaging with the CCD, since there is no inherent microsecond-level triggering capability. Exposure time was set to 0.1, 1.0, and 3.0 s; longer exposure times resulted in partial saturation of the chip. The grayscale CCD data were processed into three descriptive composite images, corresponding to each of the tested exposure times, following the same steps as outlined for the CMOS camera above.

2.C.2. Intensified detectors: ICCDs and EM-ICCD

The biggest distinction between acquisition, using the two standalone detectors and the three intensified detectors, was the ambient room light conditions; the former required all room lights be turned off, while the latter allowed for soft lighting from incandescent bulbs throughout the room. This distinction arises from the triggering and submicrosecond gating capabilities of the intensifier. A software package called LightField (Princeton Instruments, Trenton, NJ) produced by the manufacturer of the intensified cameras allowed for extensive control of gain, time-gating, and acquisition settings and was used to acquire all images on the intensified detectors.

Since the Linac delivers radiation as a series of pulses at a frequency dependent on the dose rate (for example, approximately 200 Hz at a dose rate of 600 MUs/min), it is possible to both synchronize (trigger) and limit image acquisition to the instant of Cherenkov emission (time gate) by using the intensifier as a picosecond-capable optical switch or shutter. Current mechanical shutters are not capable of achieving the small time-scale triggering and gating that the intensifier inherently provides and is necessary for this application.

For the photon beam described above, intensified image acquisition is restrained to a window which starts 0.027 μs after the trigger signal is received (the smallest trigger gate delay supported by the tested cameras) and stays open for 3.25 μs; these values are specified in the acquisition software LightField and based off of Monte Carlo simulations regarding the duration of Cherenkov photon emission.[25] The trigger signal originates from the Linac as the current on the x-ray target (a roughly 200 Hz signal), which is accessible as a voltage on the Linac stand compartment through a BNC connection; the trigger threshold in this case was set to -0.5 V. The trigger voltage threshold can vary based on the make, model, and mode of the Linac being used.

The triggering and gating of image acquisition allowed the intensified cameras to only capture data in the microsecond windows when Cherenkov photons were being emitted from the surface, as opposed to continuous acquisition as was the case for the standalone detectors. Each Linac pulse triggered the image intensifier to turn on for the prescribed gate window, and provided the signal for one accumulation of data on the CCD chip.

Once the set number of accumulations on chip was aggregate on the detector, the image was readout to software. The readout process took the most time, and it created the camera-specific limit on maximum supportable frame-rate. In the case of the ICCDs, this was 12.9 fps using the full resolution of the chip. Beyond readout time, the frame rate of data acquisition was dependent on how many on-chip accumulations were desired for each frame before readout. The triggering and gating process is described in further detail in previous publications.[25]

Subsequently, instead of varying the exposure time to adjust the frame rate as was the case for the standalone detectors, frame rate for the intensified cameras was more appropriately adjusted by varying the number of on-chip accumulations before the image was read off of the sensor. Table II outlines the trade-off between on-chip accumulations and frame rate, as exhibited by the two ICCDs tested, without image binning; binning can increase the possible frame rate at the expense of reducing spatial resolution. In the case of relatively low number of on-chip accumulations, the readout time of the camera (approximately 70 ms with 1024×1024 resolution) will limit the frame rate. Because a different sensor with lower resolution (512×512) is used in the EM-ICCD, it is able to achieve 30 fps at one on-chip accumulation, without binning.

The ICCDs, which vary primarily in the quantum efficiency spectra of their intensifiers (Unigen 2 vs HRf) and camera generation from the manufacturer (PIMAX3 vs PIMAX4), acquired 100 Cherenkov images and 10 background images at each of the frame rates listed in Table II, at maximum gain setting of 100. However, while condensing the full data set to a single exemplary image for each setting, the number of frames processed was limited to the number of frames that could be acquired in 7.75 s, the time it takes to obtain 100 images at a rate of 12.9 fps with the ICCDs; the number of frames was then rounded down to avoid introducing partial frames. This technique was implemented during analysis to ensure that the slower frame rates did not receive any artificial

TABLE II. Selected number of on-chip accumulations and associated readout frame rate for the two ICCD cameras (PIMax3 1024i and PIMax4 1024i) when using full chip acquisition (no binning). The number of analyzed frames was varied to reflect a constant overall time of acquisition.

On-Chip Accumulations	1	5	10	15	20	25	30	35	40	45	50	75	100	200
Frames per second	12.9	11.3	9.73	8.57	7.66	6.92	6.32	5.81	5.37	5	4.68	3.53	2.83	1.59
Analyzed frames	100	88	75	66	59	54	49	45	42	39	36	27	22	12

inflation from the benefit of longer aggregate exposure times to the Cherenkov signal. By keeping the acquisition time of each data set constant through coordinating the number of frames analyzed with the frame rate, a better relative comparison of performance was established between the various acquisition settings investigated.

The EM-ICCD was tested using various configurations, however, the most pertinent for this study was set up at one on-chip accumulation (30 fps), at a set gain factor of 10 000 between the intensifier (21.54×) and the electron multiplier (464.16×), which were the manufacturer-provided optimized gain settings. It is worthwhile to note that these optimized settings were established for a different imaging application in a separate laboratory environment, and is not necessarily representative of the most advantageous configuration for Cherenkov imaging.

Processing of the images acquired by the ICCDs and EM-ICCD was carried out in the same fashion as the standalone detectors. The median of the stack of Cherenkov images was calculated (with the stack size being the number of images listed in Table II for the ICCDs and 100 images for the EM-ICCD). The average of the background images was subtracted from the median and an 11×11 spatial median was applied.[30]

2.D. Metric of performance

Imaging systems which are used in low signal levels, especially where photon counting is a factor, are typically dominated by Poisson distributed shot noise from the probability of detection leading to a distribution of measured values, where the mean is N and the standard deviation or noise is $N^{1/2}$. In this situation, the signal to noise ratio is thus simply $N^{1/2}$. Overlaid on this noise are the electronic readout noise, spatial noise, and any bias errors from background or background subtraction. In this application, there is the addition of salt-and-pepper noise from the random introduction of individual scatter events causing extremely high values at individual clusters of pixels. The combined removal of the salt-and-pepper through temporal median filtering together with the background subtraction leads to data from different cameras which must be compared quantitatively.

The ideal comparator for medical systems such as this is typically the DQE, which is formally defined as the ratio of the quanta signal measured to the quanta signal input. Since the input or output quantum signal is simply measured as the square of the signal to noise ratio (SNR), then the DQE at zero spatial frequency, can be expressed as

$$\mathrm{DQE}(0) = N_{\mathrm{OUT}}/N_{\mathrm{IN}} = (\mathrm{SNR}_{\mathrm{OUT}})^2/(\mathrm{SNR}_{\mathrm{IN}})^2.$$

The problem in using this expression to compare Cherenkov signals is that the Cherenkov signal input $(\mathrm{SNR}_{\mathrm{IN}})^2$ would need to be independently measured by another system. Since the Cherenkov signal is itself very low fluence, broadband spectrum, it is a challenge to quantify. Additionally, most low sensitivity optical detectors are substantially corrupted in the high radiation environment of a therapy room, so the ability to directly measure N_{IN} is very challenging. However, if cameras are compared with a fixed lens and fixed geometry for imaging, then N_{OUT} measured is directly proportional to the DQE. As such, in this study, we show the results as N_{OUT} or $(\mathrm{SNR}_{\mathrm{OUT}})^2$ for inter-camera comparisons. In the data processing presented here, the SNR was calculated as the average intensity value of the analyzed region, $\bar{\mu}_{\mathrm{ROI}}$ divided by the standard deviation of that region, σ_{ROI}

$$\mathrm{SNR} = \frac{\bar{\mu}_{\mathrm{ROI}}}{\sigma_{\mathrm{ROI}}}.$$

3. RESULTS

3.A. Standalone detector results

Figure 2 shows the processed images from the tested CMOS and CCD cameras, with varying lengths of image exposure. Processing of all presented images included temporal median filtering, background subtraction, as well as spatial median filtering, as described in Sec. 2.C. The CMOS images are represented in double format (with values ranging from 0 to 1), while the CCD images are in 16-bit format (values from 0 to 65 535), which affects the interpretation of the value ranges of their respective colorbars. This distinction arises from the native format of the raw data files.

3.B. Intensified detector results

3.B.1. Phantom study results

Figure 3 shows several key imaging results of the three intensified cameras, processed using the methods detailed in Sec. 2.C. The two columns show three images each that characterize the detected signal at 12.9 (maximum for this detector because of the image readout time from the chip), 9.7, and 4.7 fps.

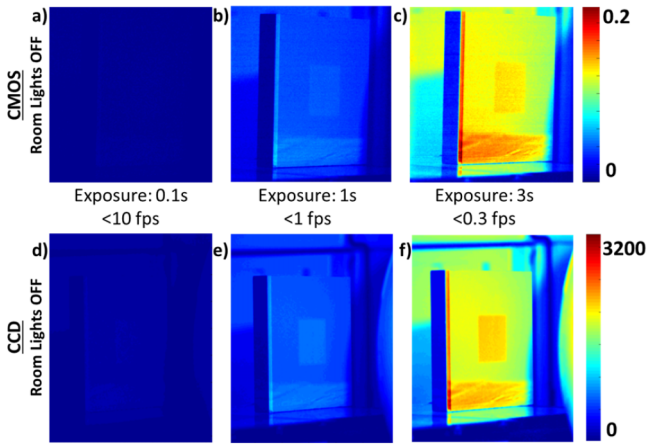

FIG. 2. Processed Cherenkov images collected using the CMOS [(a)–(c), top row on the same intensity scale] and CCD [(d)–(f), bottom row on the same intensity scale] cameras with varying exposure times. Room lights were off, since there is no mechanism of fast triggering and gating available with these two camera options. Note the Cherenkov signal was low relative to the background room light. At long exposure times with room lights off, a modest contrast is seen. Their utility is feasible, but only at low frame rates (below 1 fps), with noticeable background in the image even after background subtraction.

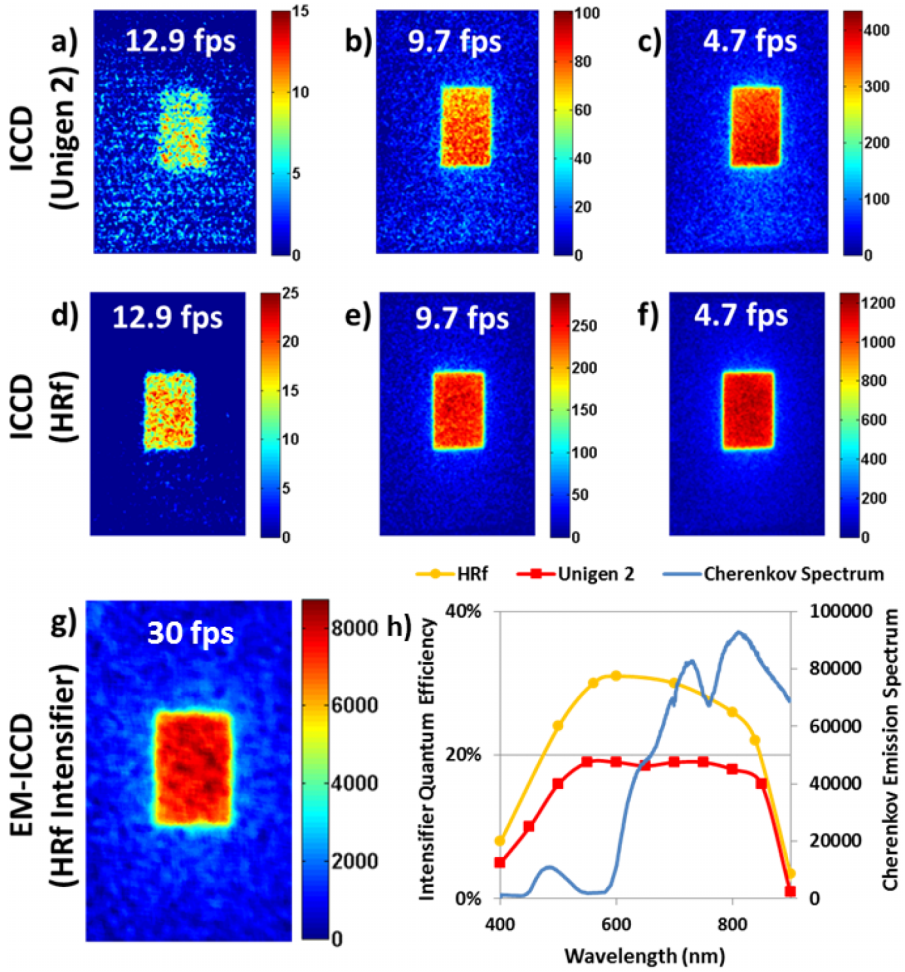

FIG. 3. Cherenkov images captured using three types of intensified cameras with room lights on are shown. The HRf ICCD (d)–(f) outperformed the Unigen 2 ICCD (a)–(c) because of overall higher intensifier quantum efficiency. However, best performance was demonstrated from a high-gain electron-multiplied CCD (g), which allowed for single-shot imaging, where a high-signal Cherenkov image can be captured from a single radiation pulse from the Linac (<0.05 cGy of dose); this image is a constructed from a temporal median filter of multiple frames following the same image processing techniques as with the ICCDs. Minor reshaping was implemented to visually negate the effect of small viewpoint angle changes between systems, but was not used in any quantitative analyses. The Cherenkov spectrum plotted in the graph shown in (h) was generated using geant4-based simulations of a 6 MV x-ray beam irradiating a light-skinned tissue volume.[21] The QE curves were plotted from data supplied by the camera manufacturer.

The bulk of the data in the original clinical trial was collected with the Unigen 2 ICCD at 4.7 fps. Figure 3(c) is thus characteristic of the minimum signal desired for an imaging sensor in this application, which is 0.56% of the full 16-bit range (an average of 369/65 536 electron counts per pixel) after processing, including background subtraction. For simplicity, 0.5% was chosen as the average intensity cutoff for adequate Cherenkov signal, which corresponds to a pixel intensity value of 327 as the minimum threshold. The images Figs. 3(c)–3(f) are from the HRf ICCD for the same frame rates.

Figure 3(g) shows the image acquired by the EM-ICCD at 30 fps, where each frame is the signal from a single radiation pulse; here, the median of 100 such frames is displayed and analyzed in accordance with the method used for the two ICCDs. This camera is specified to a higher maximum frame rate, because the readout time of the chip is shorter as a result of the lower overall resolution (512×512 as opposed to 1024×1024). The average Cherenkov intensity of the beam region of interest (here, only 60×100 pixels, again because of the overall decreased resolution of the EM-ICCD to 512×512 pixels) was over 20 times the defined minimum threshold for adequate imaging (0.5% or 327 counts).

Initial visual inspection of these images indicates enhanced performance from the HRf intensifier as compared to the Unigen 2 for the ICCDs. Likewise, the EM-ICCD produced a high-intensity image at the fastest frame rate, due to the increased, dual-faceted amplification capabilities of the hardware.

The manufacturer-provided quantum efficiency curves for the intensifiers are reproduced in Fig. 3(h), alongside the relative number of Cherenkov photons emitted from tissue at each wavelength. The latter curve was generated from a geant4-based simulation in GAMOS (Ref. 31) of a 6 MV, 10×10 cm x-ray beam at SSD = 100 cm irradiating a volume with optical properties consistent with those found in the literature for a light-skinned sample, as published in previous work.[21] The Cherenkov photon count in the y-axis of the

spectrum corresponds to delivery of 1 Gy of dose to the entire tissue volume. Quantitative analysis of the treatment regions corroborated the initial qualitative inspections. Figure shows the complete set of data points for the two ICCD cameras.

The HRf ICCD SNR^2 values are shown for each of the tested frame rates, for both lights on and lights off. These surpassed the SNR^2 of the Unigen 2 ICCD at 4.7 fps, except in the case of imaging at 12.9 fps. All frame rates except for the maximum possible for the Unigen 2 ICCD (12.9 fps) exceeded a SNR of 5, and so were considered acceptable for further analysis in terms of overall useful signal. This threshold is somewhat arbitrary, but provides a decision point to compare camera performance at a reasonable, yet modest SNR value, and is based upon the Rose criterion for the average threshold for visual detection of signals.

The orange highlighted region of the graph in Fig. 4(c) indicates the region of acceptable average Cherenkov intensity values – those at or above the Unigen 2 ICCD detected intensity from the phantom under the same imaging conditions as the first clinical trial (0.5% of the bit depth or 327 counts). Following this guideline, 8.6 fps is the maximum frame rate recommended for clinical Cherenkov image acquisition using the HRf ICCD camera to maintain previously established levels of signal. This graph further illustrates the effectiveness of the imaging and processing technique in eliminating the effects of ambient room lighting. Both cameras exhibit a calculated Pearson correlation coefficient of $r = 0.9999$ when comparing the average intensity values with lights on versus with lights off.

The SNR^2_{IN} and average Cherenkov intensity for the EM-ICCD are not shown on this graph to maintain clarity, since they were measured at over twice the frame rate as the maximum ICCD acquisitions. These values are provided in Table III. Again, the lights in the room did not noticeably affect the measurement. It is critical to note that the average Cherenkov intensity for the EM-ICCD was almost twice the largest measured intensity captured by the HRf ICCD and five times that of the Unigen 2 ICCD. A metric which would be useful in evaluating camera performance, but is not included in this analysis, is DQE. This quantity is directly proportional to the measured SNR^2, and so this has been shown in the table.

3.B.2. Clinical image comparison

To more fully evaluate the effect of the resolution limitation of the EM-ICCD, it is useful to reference the clinical patient images acquired with the EM-ICCD and qualitatively compare them to the other images from the clinical trial, which were acquired with the Unigen 2 ICCD. Figure 5 depicts these images, which for the EM-ICCD [Figs. 5(a) and 5(c)] were acquired at 30 fps (from a single radiation pulse) on patient A, and for the Unigen 2 ICCD [Figs. 5(b) and 5(d)] were acquired at 4.7 fps on patient B. These single, processed images are the composite sum over the course of a single day's treatment for each patient. Because the camera is stationary, both entrance and exit profiles of the beam are imaged on the patients' surface, depending on the gantry angle with respect to the camera position.

When comparing the intensity-mapped images of the EM-ICCD [Fig. 5(a)] and the Unigen 2 ICCD [Fig. 5(b)], it is evident that the latter is much smoother in appearance, simply

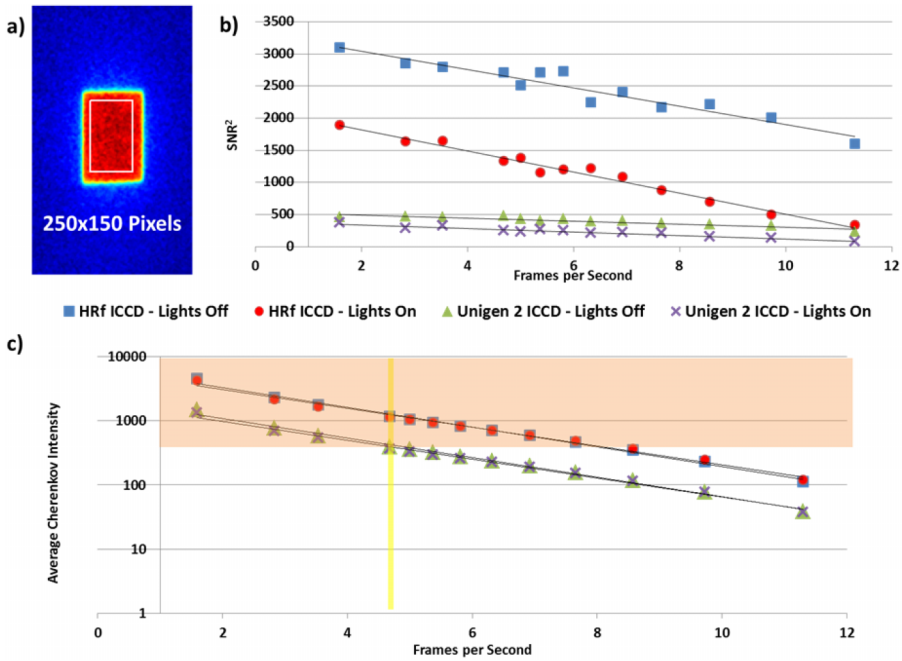

FIG. 4. Quantitative analysis of a 250×150 pixel region shown in (a) for the ICCDs within the incident beam looks at the square of the signal to noise ratio in the region (b) and average Cherenkov intensity in the region (c) versus acquisition frame rate. The yellow vertical line in graph (c) highlights Unigen 2 performance at 4.7 fps, which is the basis for performance comparison (above 0.5% of the bit depth or 327 counts). Intensity values that fall in the orange region of the chart qualify as adequate signal under this defined metric.

TABLE III. Average Cherenkov intensity and signal to noise ratio values for the EM-ICCD imaging at 30 fps.

EM-ICCD – 30 Frames per second					
Lights off			Lights on		
Average Cherenkov intensity	SNR	SNR^2	Average Cherenkov intensity	SNR	SNR^2
7377	35.6	1270	7716	34.5	1190

because the physical pixel sizes are smaller and there are more of them. The lower resolution (512×512 as compared to 1024×1024) and larger physical pixel size (16.0×16.0 μm as opposed to 12.8×12.8 μm) of the EM-ICCD versus the Unigen 2 ICCD contributes to the blockier, less-smooth Cherenkov intensity pattern in Fig. 5(a). This mismatch in the pixel count between the two cameras was unfortunate and makes it less useful to directly compare them based upon spatial resolution standards, so here, we largely focus on the frame rate performance characteristics given the relative gain differences in the two systems.

It is possible to detect the blood vessels in the Cherenkov images, because there is a difference in the attenuation coefficients between the breast tissue and the blood vessels, allowing for observed contrast in the images. After comparing the grayscale images [Figs. 5(c) and 5(d)], it is visually apparent that the lowered resolution does not hinder the detection of these blood vessels.

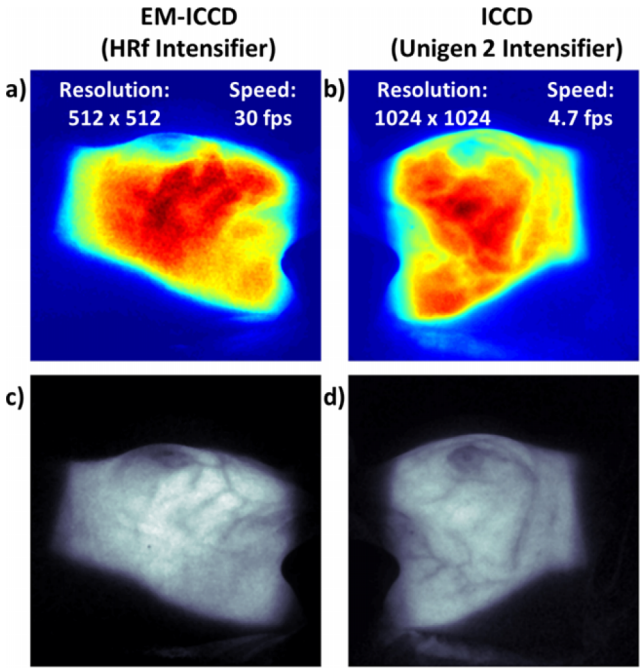

FIG. 5. *In vivo* Cherenkov images captured during whole-breast irradiation of two patients. The left column shows images captured on the EM-ICCD (a) and (c) and the right column shows images from the Unigen 2 ICCD (b) and (d). All images are self normalized. Images (a) and (b) are presented using an intensity colormap, and research is being done to correlate relative intensity to surface dose. Images (c) and (d) are the same processed images as (a) and (b), respectively, only shown in grayscale, where it is easier to visually distinguish the appearance of the blood vessels.

4. DISCUSSION

Overall, five cameras were investigated in this study to get a better understanding of the hardware requirements of detectors for clinical Cherenkov photon imaging during radiotherapy. The decision of camera type depends on the specific application of Cherenkov imaging (clinical or quality assurance) and the importance of three main criteria to that application*: (i) low light sensitivity, (ii) background light suppression, and (iii) fast frame rate.* The decision process for using different cameras based upon their strengths and limitations is outlined in Fig. 6.

Video frame rates are required in dynamic therapies, where the beam shape is changing, and in patient scenarios, so that the duration of the treatment is captured. Beyond that criterion, the camera selection will depend upon lighting conditions in the imaging environment. While an electron-multiplying charge coupled device (EMCCD) was not directly tested for this investigation, it has been used by other groups,[32] and the gain would logically allow for higher frame rates than possible with a standalone camera. However, as it does not have an external hardware intensifier component specifically, it lacks the inherent ability to time-gate on the microsecond level required for imaging with room lights on, as was demonstrated in this study using two ICCDs and an EM-ICCD.

Visual inspection of the processed images from the two standalone detectors (CMOS and CCD), shown in Fig. 2, clearly demonstrated the ineffectiveness of these cameras for imaging Cherenkov from tissue. Not only are the room lights

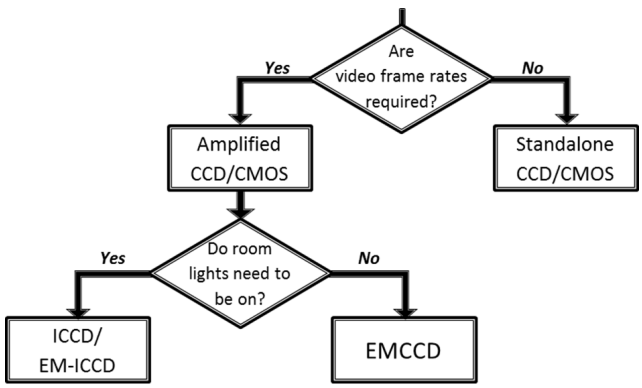

FIG. 6. Decision flow chart for camera selection in Cherenkov imaging. Since clinical imaging requires both fast frame rates and ambient room light for patient safety, an intensified, time-gated solution is required. Other cameras can be used for quality assurance applications with room lights off, over longer acquisition intervals.

off for these cases, a condition that is not ideal for patient safety or comfort, but also the exposure time required to properly resolve the Cherenkov signal is too large to support real-time imaging, which is the overarching goal of a clinical imaging system.

Since the contrast between the Cherenkov signal and the background (the rest of the phantom surface) is not qualitatively adequate even under what would be considered optimal imaging conditions with the room lights off, it can be concluded that the CMOS and CCD detectors are not adequate for imaging tissue real-time. While it is possible to image optically transparent, less absorptive media such as water or fluorescent molecule doped water using these types of detectors,[21] CMOS and CCD cameras are simply not viable as standalone sensors for imaging Cherenkov emission real-time from tissue.

Standalone detectors do not have any means of signal amplification, so there is not currently a simple method of triggering and time gating on the microsecond time scale with them, and absorption of the Cherenkov emission by tissue diminishes the signal to below any reasonable noise floor or resolvable contrast. These cameras still have a place for Cherenkov imaging if speed is not an issue, room lights can be off, and the dielectric medium is transparent to the majority of the Cherenkov spectrum. Notably, they are still suited for quality assurance applications.[19,20,33,34]

With the standalone detectors sufficiently disproven of viability as real-time Cherenkov imaging cameras of tissue (at least without substantial custom modifications), focus was shifted to the intensified cameras. Between the gain and the ability to trigger, the two ICCD cameras and EM-ICCD were more sensitive to the Cherenkov signal, and could adequately detect the emission from tissue even with ambient room lights.

The superior performance of the HRf ICCD as compared to the Unigen 2 intensifier is attributed to the higher quantum efficiency of the HRf intensifier. It is for this reason that the quantum efficiency of a camera system for incoming photons in the 600–800 nm range must be taken into consideration when determining suitability of a camera system for Cherenkov imaging. It is predominantly these wavelengths that escape the tissue, since tissue preferentially attenuates lower optical wavelengths, and thus absorbs the more widely known "Cherenkov blue" optical emission.

The EM-ICCD definitively outperformed all other cameras examined in this study for performance at clinical Cherenkov imaging in terms of both speed and sensitivity. The increase in gain factor from having two amplification mechanisms instead of just one (i.e., from the intensifier and electron multiplier) allowed the EM-ICCD to demonstrate single-shot imaging. Single-shot imaging is accomplished when the Cherenkov emission from a single radiation pulse (a single on-chip accumulation) is adequate for imaging. The only specification where the EM-ICCD falls behind the others is in resolution (512×512 as compared to 1024×1024 for the ICCDs).

The implication of single-shot imaging is the potential to measure the treatment region and detect abnormalities from a single radiation pulse, which typically delivers less than 0.05 cGy of dose in the volume for the given beam. For a real-time treatment verification system, finding errors with minimal dose improperly delivered is ideal. If the beam shape or intensity map on the patient can be registered to a gold standard for that treatment, deviations from the intended plan could hypothetically be observed after a single radiation pulse, and alert the clinician to the problem immediately upon starting the treatment or encountering the error.

In the clinical images, both cameras implemented clinically were able to resolve the blood vessels in the breast. We propose these patterns offer patient-specific, unique markings in the Cherenkov images which could be used to more accurately track patient alignment and movement, especially in the nonrigid region of the breast.[24] The 30 fps acquisition rate of the EM-ICCD, where all of the Cherenkov signal per frame is recovered from a single radiation pulse from the Linac, provides an advantage over the slower, 4.7 fps acquisition rate of the Unigen 2 ICCD (a sum of 50 radiation pulses); not only is the dose delivered per frame much lower for the EM-ICCD but also the hypothetical time cost of error detection is much shorter.

Since the resolution limitation does not hinder blood vessel detection, the fast frame rate of the EM-ICCD makes it an ideal candidate for research in clinical Cherenkov imaging, if cost is not an obstacle. The HRf ICCD offers an acceptable, lower cost alternative. In general, a camera intended for clinical Cherenkov imaging should have a method of gated acquisition on the microsecond level, and a mechanism of light amplification. Best performance will then be a trade-off in factors of resolution, speed, and contrast.

5. CONCLUSIONS

All data collected for this study supported the hypothesis that a time-gated, gain equipped system is required for real-time Cherenkov imaging of patients with ambient room lights. Standalone camera systems such as CMOS and CCD cameras, while adequate for quality assurance applications, do not perform fast enough for a real-time system, and are not sensitive enough to the diminished signal from absorptive tissue.

Each of the three intensified cameras tested could successfully image Cherenkov emission from the solid water phantom at video rates. The Unigen 2 ICCD exhibited only basic performance, since the older generation intensifier was in general not as sensitive to the optical Cherenkov spectrum. The HRf ICCD proved to be the mid-grade option, since the wavelength-dependent quantum efficiencies of the intensifier were higher than the Unigen 2 intensifier, and satisfactorily aligned with the Cherenkov emission spectrum from tissue. The EM-ICCD demonstrated the best performance, and established the viability of imaging from a single pulse of x-rays from the linear accelerator.

Camera selection for both clinical Cherenkov imaging and quality assurance Cherenkov imaging is a nontrivial task, dependent on many factors, and it is a challenge to compare devices from different manufacturers given subtleties of the specifications provided. When looking to implement a system, one needs to determine imaging priorities. However,

to accomplish video-rate image acquisition with room lights on for patient comfort and safety, it is necessary to find a gated solution with some form of signal amplification. Gating will ensure Cherenkov photon detection amidst ambient room lighting, and the level of amplification will decrease the overall length of acquisition needed to attain video-rate image streaming.

ACKNOWLEDGMENTS

This study has been funded by NIH Grant Nos. R21EB-17559 and R01CA109558 as well as Norris Cotton Cancer Center Pilot funding. The authors would like to thank Manjul Shah from Princeton Instruments for very useful discussions in the implementation and analysis of this work.

[a]Authors to whom correspondence should be addressed. Electronic addresses: Jacqueline.M.Andreozzi.th@dartmouth.edu and Brian.W.Pogue@dartmouth.edu

[1]A. Ruggiero, J. P. Holland, J. S. Lewis, and J. Grimm, "Cerenkov luminescence imaging of medical isotopes," J. Nucl. Med. **51**(7), 1123–1130 (2010).

[2]B. Mijnheer, S. Beddar, J. Izewska, and C. Reft, "In vivo dosimetry in external beam radiotherapy," Med. Phys. **40**(7), 070903 (19pp.) (2013).

[3]E. J. Bloemen-van Gurp, B. J. Mijnheer, T. A. M. Verschueren, and P. Lambin, "Total body irradiation, toward optimal individual delivery: Dose evaluation with metal oxide field effect transistors, thermoluminescence detectors, and a treatment planning system," Int. J. Radiat. Oncol., Biol., Phys. **69**(4), 1297–1304 (2007).

[4]L. G. Pacyna, M. Darby, and K. Prado, "Use of thermoluminescent dosimetry to verify dose compensation in total body irradiation," Med. Dosim. **22**(4), 319–324 (1997).

[5]M. A. Duch, M. Ginjaume, H. Chakkor, X. Ortega, N. Jornet, and M. Ribas, "Thermoluminescence dosimetry applied to in vivo dose measurements for total body irradiation techniques," Radiother. Oncol. **47**(3), 319–324 (1998).

[6]F. Sánchez-Doblado, J. A. Terrón, B. Sánchez-Nieto, R. Arráns, L. Errazquin, D. Biggs, C. Lee, L. Núñez, A. Delgado, and J. L. Muñiz, "Verification of an on line in vivo semiconductor dosimetry system for TBI with two TLD procedures," Radiother. Oncol. **34**(1), 73–77 (1995).

[7]P. Mangili, C. Fiorino, A. Rosso, G. M. Cattaneo, R. Parisi, E. Villa, and R. Calandrino, "In-vivo dosimetry by diode semiconductors in combination with portal films during TBI: Reporting a 5-year clinical experience," Radiother. Oncol. **52**(3), 269–276 (1999).

[8]R. Weaver, B. Gerbi, and K. Dusenbery, "Evaluation of dose variation during total skin electron irradiation using thermoluminescent dosimeters," Int. J. Radiat. Oncol., Biol., Phys. **33**(2), 475–478 (1995).

[9]S. J. Blake, A. L. McNamara, S. Deshpande, L. Holloway, P. B. Greer, Z. Kuncic, and P. Vial, "Characterization of a novel EPID designed for simultaneous imaging and dose verification in radiotherapy," Med. Phys. **40**(9), 091902 (11pp.) (2013).

[10]K. Chytyk-Praznik, E. van Uytven, T. A. van Beek, P. B. Greer, and B. M. C. McCurdy, "Model-based prediction of portal dose images during patient treatment," Med. Phys. **40**(3), 031713 (11pp.) (2013).

[11]T. Fuangrod, H. C. Woodruff, E. van Uytven, B. M. C. McCurdy, Z. Kuncic, D. J. O'Connor, and P. B. Greer, "A system for EPID-based real-time treatment delivery verification during dynamic IMRT treatment," Med. Phys. **40**(9), 091907 (11pp.) (2013).

[12]M.-H. Lin, J. Li, L. Wang, S. Koren, J. Fan, E. Forkal, and C.-M. Ma, "4D patient dose reconstruction using online measured EPID cine images for lung SBRT treatment validation," Med. Phys. **39**(10), 5949–5958 (2012).

[13]N. Naiyanet, S. Oonsiri, C. Lertbutsayanukul, and S. Suriyapee, "Measurements of patient's setup variation in intensity-modulated radiation therapy of head and neck cancer using electronic portal imaging device," Biomed. Imaging Intervention J. **3**(1), e30 (7pp.) (2007).

[14]R. L. Smith, M. L. Taylor, L. N. McDermott, A. Haworth, J. L. Millar, and R. D. Franich, "Source position verification and dosimetry in HDR brachytherapy using an EPID," Med. Phys. **40**(11), 111706 (12pp.) (2013).

[15]S. Steciw, B. Warkentin, S. Rathee, and B. G. Fallone, "Three-dimensional IMRT verification with a flat-panel EPID," Med. Phys. **32**(2), 600–612 (2005).

[16]W. van Elmpt, L. McDermott, S. Nijsten, M. Wendling, P. Lambin, and B. Mijnheer, "A literature review of electronic portal imaging for radiotherapy dosimetry," Radiother. Oncol. **88**(3), 289–309 (2008).

[17]H. C. Woodruff, T. Fuangrod, P. Rowshanfarzad, B. M. C. McCurdy, and P. B. Greer, "Gantry-angle resolved VMAT pretreatment verification using EPID image prediction," Med. Phys. **40**(8), 081715 (9pp.) (2013).

[18]S. L. Berry, C. Polvorosa, S. Cheng, I. Deutsch, K. S. C. Chao, and C.-S. Wuu, "Initial clinical experience performing patient treatment verification with an electronic portal imaging device transit dosimeter," Int. J. Radiat. Oncol., Biol., Phys. **88**(1), 204–209 (2014).

[19]A. K. Glaser, J. M. Andreozzi, S. C. Davis, R. Zhang, B. W. Pogue, C. J. Fox, and D. J. Gladstone, "Video-rate optical dosimetry and dynamic visualization of IMRT and VMAT treatment plans in water using Cherenkov radiation," Med. Phys. **41**(6), 062102 (9pp.) (2014).

[20]R. Zhang, A. K. Glaser, D. J. Gladstone, C. J. Fox, and B. W. Pogue, "Superficial dosimetry imaging based on Čerenkov emission for external beam radiotherapy with megavoltage x-ray beam," Med. Phys. **40**(10), 101914 (12pp.) (2013).

[21]A. K. Glaser, R. Zhang, D. J. Gladstone, and B. W. Pogue, "Optical dosimetry of radiotherapy beams using Cherenkov radiation: The relationship between light emission and dose," Phys. Med. Biol. **59**(14), 3789–3811 (2014).

[22]L. A. Jarvis, R. Zhang, D. J. Gladstone, S. Jiang, W. Hitchcock, O. D. Friedman, A. K. Glaser, M. Jermyn, and B. W. Pogue, "Cherenkov video imaging allows for the first visualization of radiation therapy in real time," Int. J. Radiat. Oncol., Biol., Phys. **89**(3), 615–622 (2014).

[23]R. Zhang, D. J. Gladstone, L. A. Jarvis, R. R. Strawbridge, P. Jack Hoopes, O. D. Friedman, A. K. Glaser, and B. W. Pogue, "Real-time in vivo Cherenkoscopy imaging during external beam radiation therapy," J. Biomed. Opt. **18**(11), 110504 (2013).

[24]R. Zhang, J. M. Andreozzi, D. J. Gladstone, W. L. Hitchcock, A. K. Glaser, S. Jiang, B. W. Pogue, and L. A. Jarvis, "Cherenkoscopy based patient positioning validation and movement tracking during post-lumpectomy whole breast radiation therapy," Phys. Med. Biol. **60**(1), L1–L14 (2015).

[25]A. K. Glaser, R. Zhang, S. C. Davis, D. J. Gladstone, and B. W. Pogue, "Time-gated Cherenkov emission spectroscopy from linear accelerator irradiation of tissue phantoms," Opt. Lett. **37**(7), 1193–1195 (2012).

[26]J. Sandell and T. Zhu, "A review of in vivo optical properties of human tissues and its impact on PDT," J. Biophotonics **4**(11-12), 773–787 (2011).

[27]S. L. Jacques, "Optical properties of biological tissues: A review," Phys. Med. Biol. **58**(11), R37–R61 (2013).

[28]J. Axelsson, A. K. Glaser, D. J. Gladstone, and B. W. Pogue, "Quantitative Cherenkov emission spectroscopy for tissue oxygenation assessment," Opt. Express **20**(5), 5133–5142 (2012).

[29]R. Zhang, A. Glaser, T. V. Esipova, S. C. Kanick, S. C. Davis, S. Vinogradov, D. Gladstone, and B. W. Pogue, "Čerenkov radiation emission and excited luminescence (CREL) sensitivity during external beam radiation therapy: Monte Carlo and tissue oxygenation phantom studies," Biomed. Opt. Express **3**(10), 2381–2394 (2012).

[30]L. Archambault, T. M. Briere, and S. Beddar, "Transient noise characterization and filtration in CCD cameras exposed to stray radiation from a medical linear accelerator," Med. Phys. **35**(10), 4342–4351 (2008).

[31]P. Arce, P. Rato, M. Cafiadas, and J. I. Lagares, "GAMOS: A geant4-based easy and flexible framework for nuclear medicine applications," *IEEE Nuclear Science Symposium Conference Record* (IEEE, Dresden, Germany, 2008), pp. 3162–3168.

[32]B. Fahimian, A. Ceballos, S. Türkcan, D. S. Kapp, and G. Pratx, "Seeing the invisible: Direct visualization of therapeutic radiation beams using air scintillation," Med. Phys. **41**(1), 010702 (6pp.) (2014).

[33]A. K. Glaser, W. H. A. Voigt, S. C. Davis, R. Zhang, D. J. Gladstone, and B. W. Pogue, "Three-dimensional Čerenkov tomography of energy deposition from ionizing radiation beams," Opt. Lett. **38**(5), 634–636 (2013).

[34]Y. Helo, I. Rosenberg, D. D'Souza, L. Macdonald, R. Speller, G. Royle, and A. Gibson, "Imaging Cerenkov emission as a quality assurance tool in electron radiotherapy," Phys. Med. Biol. **59**(8), 1963–1978 (2014).